Enhancement of fusion reactivities using non-Maxwellian energy distributions

Ben I. Squarer,[1] Carlo Presilla,[2,3] and Roberto Onofrio[1]
[1]*Department of Physics and Astronomy, Dartmouth College, 6127 Wilder Laboratory, Hanover, New Hampshire 03755, USA*
[2]*Dipartimento di Matematica, Sapienza Università di Roma, Piazzale Aldo Moro 2, Roma 00185, Italy*
[3]*Istituto Nazionale di Fisica Nucleare, Sezione di Roma 1, Roma 00185, Italy*

(Received 2 October 2023; accepted 11 January 2024; published 9 February 2024)

We discuss conditions for the enhancement of fusion reactivities arising from different choices of energy distribution functions for the reactants. The key element for potential gains in fusion reactivity is identified in the functional dependence of the tunneling coefficient on the energy, ensuring the existence of a finite range of temperatures for which reactivity of fusion processes is boosted with respect to the Maxwellian case. This is shown using a convenient parametrization of the tunneling coefficient dependence on the energy, analytically in the simplified case of a bimodal Maxwell-Boltzmann distribution, and numerically for kappa distributions. We then consider tunneling potentials progressively better approximating fusion processes and evaluate in each case the average reactivity in the case of kappa distributions.

DOI: 10.1103/PhysRevE.109.025207

I. INTRODUCTION

The relevance of controlled nuclear fusion in the current context, to contain global warming and to mitigate geopolitical conflicts, has been extensively debated. While the gap between experimental demonstrations and commercial use of nuclear fusion is being progressively narrowed with projects like ITER currently under construction, and DEMO, in the middle of this century, there have been parallel efforts to discuss the possibility to enhance fusion cross sections by exploiting the basic physics of tunneling and the possible presence of screening of the Coulomb barrier. Considering the extreme sensitivity of quantum tunneling to the details of the process, significant gains may be expected. Examples of proposals range from discussion of correlated states [1], interference from superposition of plane waves [2], use of generalized Gaussian wave packets [3,4], shielding of strong electromagnetic fields [5], and the effect of the hypothetical presence of strong scalar fields [6], among the many proposals. Another sequel of proposals has focused on the intrinsic three-dimensional nature of the confined plasmas, with the goal to enhance the reactivity by producing Maxwell-Boltzmann (MB) distributions with different temperatures along different spatial directions [7–12].

In this paper we discuss the impact of various choices of macroscopic states for the reactants, i.e., their energy distribution, on the resulting average reactivity. Preliminary discussions of this aspect can be found in Ref. [13] using Dagum distributions, and in Ref. [14], in which the potential gain in using energy distributions with hard high-energy tails of the so-called kappa distributions (κ distributions in the following)—already broadly used in space plasma physics and astrophysics [15–18]—has been discussed by evaluating reactivities with empirically determined fusion cross sections [19]. We extend here these considerations to analytically evaluated *ab initio* cross sections, showing general features and discussing conditions under which gains are expected with respect to Maxwell-Boltzmann (MB) energy distributions. A recent paper is also exploring, on top of trapping anisotropies, κ distributions in magnetically confined plasmas [20].

The paper is organized as follows: In Sec. II we first recall general properties of two classes of non-MB distributions: bimodal MB and κ distributions. We discuss the presence of population excesses at low and high energy and population depletion at intermediate energies with respect to a Maxwell-Boltzmann distribution. We then report, in Sec. III, average reactivities gains in an idealized case of tunneling coefficient dependence on the energy. In Sec. IV we discuss tunneling in the case of two barriers which are amenable to a complete analytic treatment, yet capturing some features of the more complex nuclear fusion case, the double square well and a generalized form of the Woods-Saxon potential. In the same section we also provide explicit examples of configurations, within these two classes of potentials, for which it is advantageous to use κ distributions. We briefly comment on the impact for fusion reactions involving deuterium-deuterium and deuterium-tritium mixtures, by using empirical cross sections already available in the literature.

In the conclusions we qualitatively comment on the potential relevance of these results in the context of magnetic confined fusion reactors. Two Appendixes, one on explicit calculations for the tunneling coefficient of the square well case and another on the discussion of the convexity of the tunneling coefficient evaluated with the Wentzel-Kramers-Brillouin (WKB) approximation in the case of two relevant barriers, complete the paper.

II. GENERALIZED ENERGY DISTRIBUTIONS

In practical settings and especially in hot plasmas, the energy distributions of the reactants is determined by classical statistical mechanics. We discuss here two energy distributions more general than the MB energy distribution, namely,

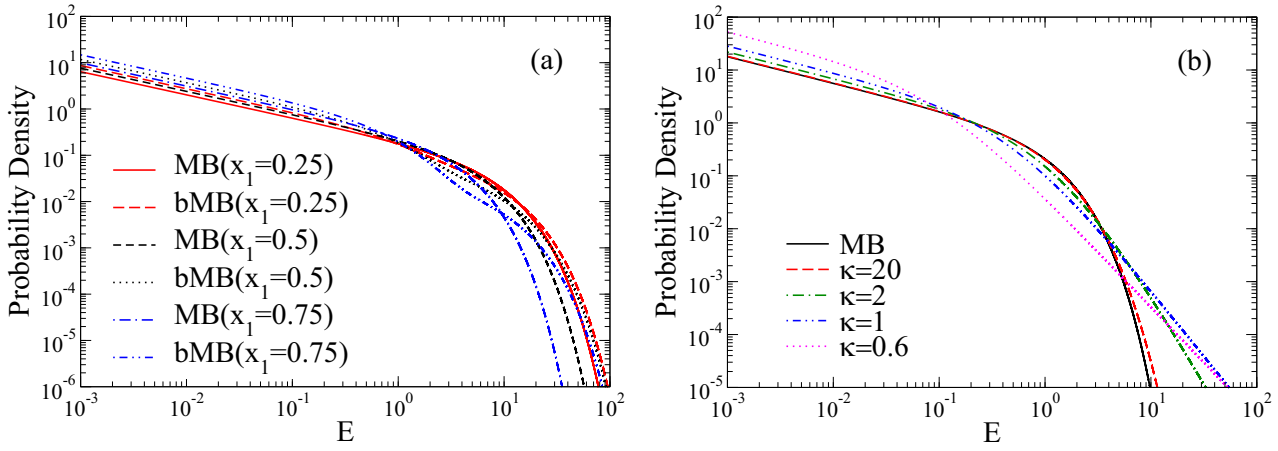

FIG. 1. Probability densities for non-Maxwell-Boltzmann energy distributions and for the corresponding MB energy distributions with the same average energy versus E (in arbitrary units). Three cases of bMB distributions are shown in panel (a), with inverse temperatures $\beta_1 = 1$ and $\beta_2 = 10^{-1}$ (in arbitrary units) for different weights of $x_1 = 0.25$, with long dashed red (light gray) line, $x_1 = 0.50$ (dotted black line), $x_1 = 0.75$ (double-dot-dashed blue line). The corresponding MB distributions with the same average energy and therefore inverse temperature β_0 [derived from Eq. (3)] are also shown $x_1 = 0.25$ with continuous red (light gray) line, $x_1 = 0.5$ (short dashed black line), $x_1 = 0.75$ (blue dot-dashed line). The case of κ distributions is shown in panel (b) for different values of $\kappa = 0.6,\ 1,\ 2,\ 20$ and constant $\eta = -1/2$. For sufficiently large κ, the distribution approaches the MB distribution. A common feature of the two non-Maxwellian distributions with respect to the corresponding MB distribution is the presence of regions with higher probability densities at both low and high energy, with a region in between for which MB instead has higher probability densities.

a superposition of two MB distributions at different temperatures and the so-called κ distribution.

The MB in one dimension is defined as

$$p_{\mathrm{MB}}(E;\beta) = \sqrt{\frac{\beta}{4\pi}} E^{-1/2} \exp\left(-\beta E\right), \tag{1}$$

with β, the unique parameter of this energy distribution, being the inverse temperature, such that the temperature T is related to β as $\beta = (k_B T)^{-1}$, with k_B the Boltzmann constant, and T expressed in Kelvin. A bimodal Maxwell-Boltzmann (bMB) distribution is described by the weighted sum of two MB distributions:

$$p_{\mathrm{bMB}}(E;\beta_1,\beta_2) = x_1 p_{\mathrm{MB}}(E;\beta_1) + x_2 p_{\mathrm{MB}}(E;\beta_2). \tag{2}$$

Here the two weights x_1 and x_2 satisfy $x_1 + x_2 = 1$, and the average energy of a bimodal system is $\langle E\rangle = x_1\beta_1^{-1} + x_2\beta_2^{-1}$. We therefore can compare a bMB distribution to a single MB distribution with the same average energy, which means with an MB distribution with inverse temperature β_0 such that

$$\beta_0^{-1} = x_1\beta_1^{-1} + x_2\beta_2^{-1}. \tag{3}$$

Examples of bMB energy distributions and comparison to the corresponding MB distributions with the inverse temperature determined by Eq. (3) are shown in Fig. 1(a). Actual bMB distributions have been observed in laboratory plasmas [21].

The class of κ distributions was introduced to fit magnetospheric electron data and have been used to describe a plethora of astrophysical and space plasmas phenomena [18]. It has been also discussed in the framework of nonextensive statistical mechanics in which the q parameter, representing nonextensivity, is shown to be related to the κ parameter [22]. Moreover, it has been shown that generalizations of bMB distributions allow us to effectively capture the effect of a κ distribution [23]. In the one-dimensional case, κ distributions can be expressed, as discussed in Ref. [24], in the following form:

$$p_\kappa(E;\beta,\kappa,\eta) = \sqrt{\frac{\beta}{4\pi(\kappa+\eta)}}\frac{\Gamma(\kappa+1)}{\Gamma(\kappa+1/2)} \times E^{-1/2}\left(1+\frac{\beta E}{\kappa+\eta}\right)^{-\kappa-1}, \tag{4}$$

in which, in addition to the inverse temperature β, two further parameters appear with respect to an MB distribution: κ and η. The parameter κ expresses the "distance" of the distribution from the corresponding MB distribution and determines more specifically the high-energy behavior due to its presence in the generalized, power-law dependent, Lorentzian function. Based on the usual definition of the exponential function as a limiting process $e^x = \lim_{n\to\infty}(1+x/n)^n$, it is evident that the MB distribution in Eq. (1) is recovered for $\kappa \to +\infty$.

For finite κ instead, the distribution has larger probability in the high-energy tail with respect to the corresponding MB distribution, and these hard tails become more prominent as κ becomes smaller. The average energy E of a particle in a κ-distributed ensemble is written as

$$E = \frac{\kappa+\eta}{\beta}\frac{\int_0^{+\infty} x^{1/2}(1+x)^{-1-\kappa}}{\int_0^{+\infty} x^{-1/2}(1+x)^{-1-\kappa}}dx = \frac{\kappa+\eta}{\beta}\frac{\Gamma(\kappa-1/2)}{2\Gamma(\kappa+1/2)} = \frac{\kappa+\eta}{2\beta(\kappa-1/2)}, \tag{5}$$

where the dimensionless parameter x is defined as $x = \beta E/(\kappa+\eta)$. Equation (5) shows that the expectation of the equipartition principle valid for an MB distribution in one dimension [$E = k_B T/2 = 1/(2\beta)$] is modified by a factor $(\kappa+\eta)/(\kappa-1/2)$, obviously tending to unity for $\kappa \to +\infty$, the MB limit. For the choice $\eta = -1/2$, the kinetic definition

of temperature valid for an MB distribution is recovered regardless of the value of κ, allowing for a fair comparison between different κ distributions therefore having the same total energy. This also coincides with the dependence of η on the number of kinetic degrees of freedom d_κ of the system (in our case $d_\kappa = 1$), as $\eta = -d_\kappa/2$ [25]. A comparison between κ and MB distributions is also possible in general at the price, however, of introducing an effective temperature depending on κ. For this reason, we focus in the following considerations only on the simplest case of $\eta = -1/2$.

Some remarks are also in order. First, the parameters T and η can be related to the velocity distribution's second moment

$$\langle v^2 \rangle = \frac{\kappa + \eta}{\kappa - 1/2} \frac{k_B T}{m}, \tag{6}$$

showing that both T and η are related to the distribution's variance (since the average velocity is zero), with the exceptional case of $\eta = -1/2$ commented above.

Second, the velocity distribution P_κ corresponding to the energy distribution p_κ as in Eq. (4), expressed as

$$P_\kappa(v;\beta,\kappa,\eta) = \sqrt{\frac{m\beta}{2\pi(\kappa+\eta)}} \frac{\Gamma(\kappa+1)}{\Gamma(\kappa+1/2)} \times \left(1 + \frac{\beta m v^2}{2(\kappa+\eta)}\right)^{-\kappa-1}, \tag{7}$$

always reaches a maximum at $v = 0$, and the ratio between the peaks of the κ distribution and the corresponding MB distribution for $v = 0$ is

$$\frac{P_\kappa(v=0;\beta,\kappa,\eta)}{P_{\mathrm{MB}}(v=0;\beta)} = \frac{\Gamma(\kappa+1)}{\sqrt{\kappa+\eta}\,\Gamma(\kappa+1/2)}. \tag{8}$$

By using asymptotic expressions for the Gamma function, for instance a Stirling-like formula (see more in general [26]),

$$\Gamma(x+1) \sim \sqrt{2\pi x}\left(\frac{x}{e}\right)^x, \tag{9}$$

we find that in the case $\eta = -1/2$ that we are considering, the ratio in Eq. (8) is always larger than unity for a finite κ, obviously tending to unity in the $\kappa \to \infty$ limit. This implies that κ distributions have both hard high-energy tails and more populated peaks at zero velocity with respect to the corresponding MB distribution. Due to the normalization of probability distributions, this implies that there will be an intermediate regime of velocities in which the MB distribution prevails over the κ distribution. This effect is shown in Fig. 1(b), in which various κ distributions are considered including the limiting case of an MB distribution, nearly indistinguishable from a κ distribution for $\kappa = 20$.

Third, an intriguing situation occurs in the limit of $\kappa \to -\eta$, as in this case, by introducing $\epsilon > 0$ such that $\kappa = -\eta + \epsilon$, we have

$$P_\kappa(v;T,-\eta+\epsilon,\eta) = \sqrt{\frac{m}{2\pi k_B T}} \epsilon^{-1/2} \frac{\Gamma(1-\eta)}{\Gamma(1/2-\eta)} \times \left(1 + \frac{m v^2}{2\epsilon k_B T}\right)^{\eta-1-\epsilon}, \tag{10}$$

which, for $\epsilon \to 0$ and in the specific case of $\eta = -1/2$ that we are considering, can be written as

$$P_\kappa(v;T,\eta,\epsilon) \simeq \frac{k_B T \epsilon}{m v^3}, \tag{11}$$

diverging in the limit of $v \to 0$ at finite ϵ.

III. REACTIVITY WITH NON-MAXWELL-BOLTZMANN DISTRIBUTIONS

In this section we provide more quantitative arguments for understanding the effectiveness of the non-Boltzmann distributions with respect to an MB distribution (for previous related discussions, see also Refs. [14,24]) for processes involving tunneling phenomena, such as fusion. Before discussing the results, it is worth commenting on this specific unusual situation in which the velocity (and kinetic energy) distribution is dominated by classical physics, yet the reactants are evolving with fully quantum-mechanical laws, either via Rutherford scattering (ineffective for nuclear fusion) or via fusion allowed by quantum tunneling. This implies that the variance of the single wave packet, so far considered as attributable to a Gaussian momentum distribution as customary for wave packets of quantum-mechanical origin, is actually determined by the spreading of the velocities due to the classical distribution in the statistical ensemble, which in turn depends on the temperature and density and the κ and η parameters in the case of a κ distribution (for a related discussion, see Ref. [27]). The cross section corresponding to the tunneling process is

$$\sigma = \frac{\pi}{k^2} T(k) = \frac{\pi \hbar^2}{2mE} T(E), \tag{12}$$

where we have introduced the wave vector k such that $\hbar k = \sqrt{2mE}$, and the velocity of the particle with wave vector k is $v = \hbar k/m$. The average reactivity is then calculated as

$$\langle \sigma v \rangle = \int_0^{+\infty} P(v) \sigma v dv = \frac{\pi \hbar^2}{\sqrt{2} m^{3/2}} \int_0^{+\infty} p(E) T(E) E^{-1/2} dE, \tag{13}$$

with $p(E)$ one of the energy distributions defined in Eqs. (1), (2), or (4).

Basically the potential gain in using non-Boltzmann distributions stems from the fact that, with respect to an MB distribution, there is a more populated high-energy tail. For the same average energy, this means that the non-Boltzmann distribution will also have a more populated low-energy component, as visible in Fig. 1. Then the advantage of using non-Boltzmann distributions relies on the functional dependence of the tunneling probability upon the energy, $T(E)$. If the latter is a convex function, the contribution to the integrated tunneling probability from the high-energy tail will overcompensate the lower contribution due to the increased component of the distribution at low energy. We also expect that, at temperature large enough there will be marginal gain in using non-Boltzmann distributions. Indeed, for an arbitrary barrier we have $T \to 1$ for $E \to +\infty$, which implies that, at high energy, the $T(E)$ curve will always be concave. We

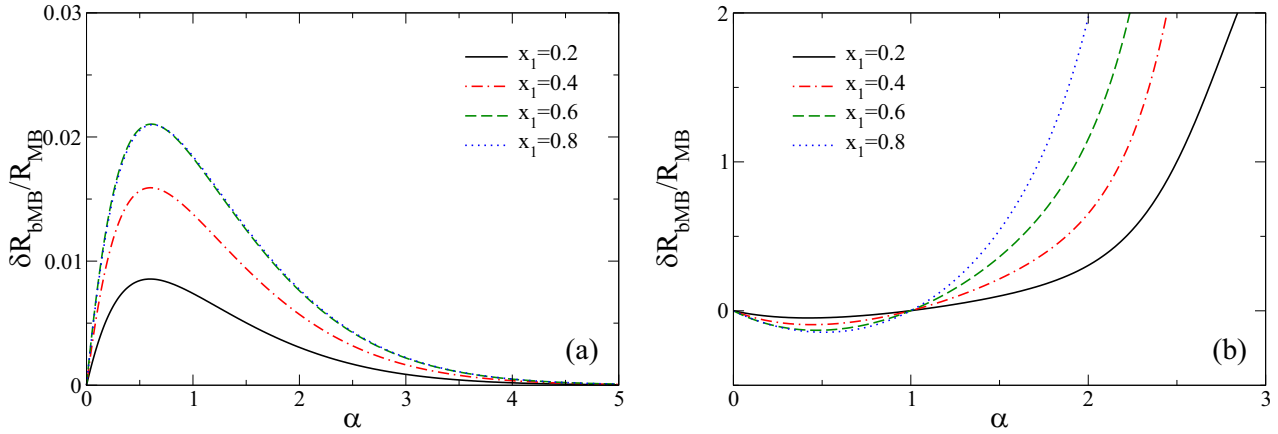

FIG. 2. Parameter $\delta R_{\rm bMB}/R_{\rm MB}$ versus the α exponent of the tunneling coefficient assumed in Eq. (15). Four cases of bMB with $x_1 = 0.2,\ 0.4,\ 0.6,\ 0.8$, all with $\beta_1 = 1$, $\beta_2 = 10^{-1}$, are depicted and (a) $\beta_0 E_0 = 10^{-2}$, (b) $\beta_0 E_0 = 10^{2}$.

therefore mainly focus on the behavior at lower temperatures, which is also the most interesting region for fusion reactions of technological interest.

For a generic non-MB distribution the gain with respect to the corresponding MB distribution may be quantified by considering the difference between the reactivities δR defined as

$$\delta R = \langle \sigma v \rangle - \langle \sigma v \rangle_{\rm MB} = \frac{\pi \hbar^2}{\sqrt{2} m^{3/2}} \int_0^{+\infty} [p(E) - p_{\rm MB}(E)] T(E) E^{-1/2} dE. \quad (14)$$

A more practical and universal dimensionless parameter is obtained by considering $\delta R/R_{\rm MB}$, the relative deviation from the MB reactivity.

In a hypothetical case of $T(E)$ scaling exactly as $E^{1/2}$ in the entire energy range, this difference will be zero because the two distributions are normalized to unity. However, the tunneling coefficient cannot grow indefinitely, being limited to unity, so this scaling law does not allow for breakeven in practice. The difference $p(E) - p_{\rm MB}(E)$ for the two cases of non-MB distributions we are considering is positive at low and high energy, being instead negative in a regime of intermediate energies, as already commented. However, at low energy the tunneling coefficient is small, while at high energy the cross section is small, as evident by the explicit $E^{-1/2}$ factor, with the tunneling coefficient approximating unity.

To put the discussion on more quantitative grounds, we introduce a fictitious tunneling coefficient depending on the energy as

$$T(x) = \begin{cases} (E/E_0)^{\alpha}, & E < E_0 \\ 1, & E > E_0. \end{cases} \quad (15)$$

The parameter α ($0 \leqslant \alpha < +\infty$) plays the role of a "convexity" parameter such that, for $E < E_0$, we have $T(E)$ convex if $\alpha > 1$, concave if $\alpha < 1$.

This allows us to obtain a simple relationship for $\delta R/R$ in the case of bMB distributions. In this case the reactivity difference δR is written as

$$\delta R_{\rm bMB} = \langle \sigma v \rangle_{\rm bMB} - \langle \sigma v \rangle_{\rm MB} = \sqrt{\frac{\pi}{2}} \frac{\hbar^2}{m^{3/2}} (x_1 F_1 + x_2 F_2 - F_0), \quad (16)$$

where

$$F_i(\beta_i; E_0, \alpha) = (\beta_i E_0)^{-\alpha} \Gamma(\alpha + 1/2; 0, \beta_i E_0) + \Gamma(\alpha + 1/2; \beta_i E_0, +\infty), \quad (17)$$

with $i = 0,\ 1,\ 2$, and

$$\Gamma(n; x, y) = \int_x^y e^{-t} t^{n-1} dt, \quad (18)$$

is the incomplete Gamma function of order n. In Fig. 2 we show the plots of $\delta R_{\rm bMB}/R_{\rm MB}$ versus α for various values of x_1 for a bMB distribution. The case (a) [Fig. 2(a)] is relative to a choice of $\beta E_0 = 10^{-2}$, case (b) [Fig. 2(b)] deals with the opposite situation of $\beta E_0 = 10^{2}$. In the limit $\beta_i E_0 \to 0$, $F_i(\beta_i; E_0, \alpha) \to \Gamma(\alpha + 1/2)$, the complete Gamma function, and then in the same limit there is complete cancellation among the three contributions, with the plot showing the small, residual term at finite $\beta_i E_0$. In the opposite limit, $\beta_i E_0 \to +\infty$, the second term on the right-hand side of (17) tends to zero, and then $F_i(\beta_i; E_0, \alpha) \to (\beta_i E_0)^{-\alpha} \Gamma(\alpha + 1/2)$. This implies a limit form of the reactivity relative difference $\delta R_{\rm bMB}/R_{\rm MB}$:

$$\frac{\delta R_{\rm bMB}}{R_{\rm MB}} \simeq \frac{x_1 \beta_1^{-\alpha} + x_2 \beta_2^{-\alpha}}{\left(x_1 \beta_1^{-1} + x_2 \beta_2^{-1}\right)^{\alpha}} - 1. \quad (19)$$

It is easy to check that, for $0 < \alpha < 1$, $\delta R_{\rm bMB}/R_{\rm MB} < 0$, and for $\alpha > 1$, $\delta R_{\rm bMB}/R_{\rm MB} > 0$, with the borderline case $\alpha = 1$ yielding $\delta R_{\rm bMB}/R_{\rm MB} = 0$. Therefore it is confirmed, at least for this power-law dependence of the tunneling coefficient upon the energy, that a convex function yields gain in using a bMB distribution with respect to an MB distribution with the same average energy. Considering the richness of possible situations, both in terms of $T(E)$ dependencies, with the possibility of resonant tunneling for instance, and of possible non-Maxwellian distributions, this result has to be considered

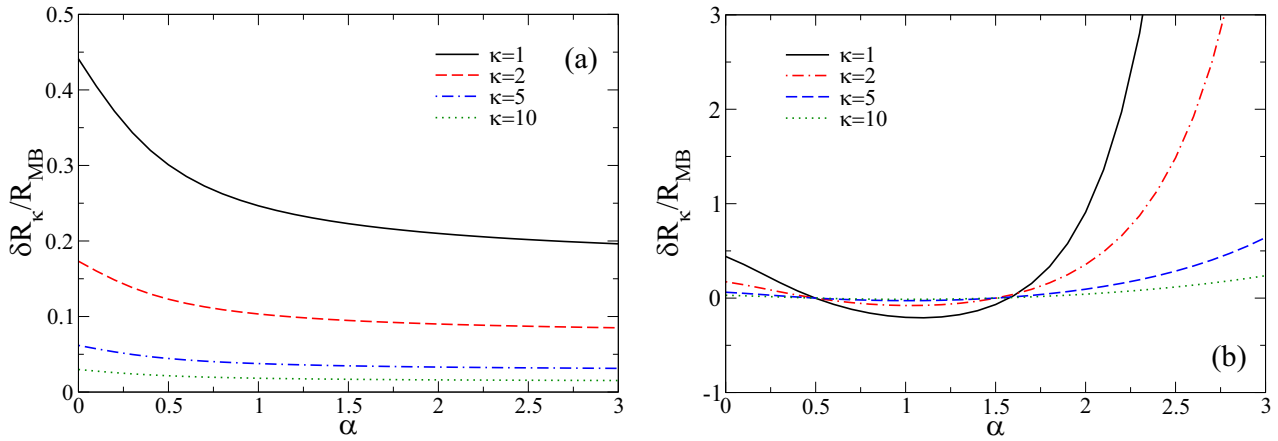

FIG. 3. Parameter $\delta R_\kappa/R_{\rm MB}$ versus the α exponent of the tunneling coefficient. Four cases are shown with $\kappa = 1, 2, 5, 10$ and (a) $\beta E_0 = 10^{-2}$, (b) $\beta E_0 = 10^2$. This plot differs from the one of bMB distributions because there is a gain in using κ distributions also at very low α and because $\delta R_\kappa = 0$ at two values of α: at $\alpha = 0.5$ independently of κ, and at a value of α progressively increasing with decreasing κ.

a qualitative guideline to appreciate the possibility of reactivity gains in a general context.

In the case of κ distributions, we write an analogous relationship

$$\delta R_\kappa = \langle \sigma v \rangle_\kappa - \langle \sigma v \rangle_{\rm MB} = \frac{\pi \hbar^2}{\sqrt{2} m^{3/2}} \int_0^{+\infty} [p_\kappa(E) - p_{\rm MB}(E)] T(E) E^{-1/2} dE, \tag{20}$$

and the numerical integration provides the plots in Fig. 3 once again for choices of $\beta E_0 = 10^{-2}$ [Fig. 3(a)] and $\beta E_0 = 10^2$ [Fig. 3(b)]. Similarly to the bMB case, when βE_0 is small there is a small enhancement at all α due to the low-energy dominance of the κ distribution with respect to the corresponding MB distribution. The case of large βE_0 is more interesting, showing an interval of α values for which the reactivity of the MB distribution is significantly larger than that of the κ distribution, which instead prevails at small and large α. The enhancement strongly depends on βE_0, and large values of this parameter, either a large E_0 or a low temperature β^{-1}, makes the reactivity quite sensitive to the high-energy tails, more prominent in the κ distribution than in the MB case. Also notice that, unlike the case of the bMB distribution, the threshold value of α for which the κ distribution has higher reactivity occurs at $\alpha > 1$, therefore requiring more curvature due to the presence of a strong low-energy component in the κ distribution and a stronger depletion at intermediate energies, as noticeable by comparing the two panels of Fig. 1.

In the specific case of the κ distribution with $\kappa \to -\eta$ discussed earlier, it is possible to support a similar convexity argument as follows: The reactivity in that case assumes the form

$$\langle \sigma v \rangle = \frac{\pi \hbar^2 k_B T \epsilon}{m} \int_0^{+\infty} \frac{T(v)}{v^4} dv, \tag{21}$$

where $T(v)$ is the tunneling coefficient $T(E)$ expressed as a function of the particle velocity, $E = mv^2/2$, and we expect $T(v) \to 1$ for $v \to +\infty$. This means that the reactivity does not present divergences at large velocities. However, there are possible divergences in the $v \to 0$ limit, depending on $T(v)$. Let us focus on the integrand at small v, including also the infinitesimal quantity ϵ for the analysis of the divergences. Let us suppose that $\epsilon \simeq v/v_0 \to 0$, i.e., goes to zero as the velocity, with v_0 a characteristic velocity, for instance the quadratic mean velocity. Then we have an expression for the reactivity as

$$\langle \sigma v \rangle \simeq \frac{\pi \hbar^2 k_B T}{m v_0} \int_0^{+\infty} \frac{T(v)}{v^3} dv. \tag{22}$$

Suppose that $T(E) \propto E^\alpha$ in the $E \to 0$ limit, then $T(v) \propto v^{2\alpha}$, which means that the integral will be finite if $\alpha > 1$, and diverging at $-\infty$ otherwise. This confirms, within the limit of this example and related assumptions, that the $T(E)$ dependence should correspond to a convex function at least initially to avoid meaningless divergences of the reactivity. Notice that, in this case, the reactivity is directly proportional to the temperature.

IV. TUNNELING COEFFICIENTS FOR POTENTIALS WITH ANALYTIC SOLUTIONS OF THE SCHRÖDINGER EQUATION

In this section, we discuss tunneling probabilities for one-dimensional systems described by potentials progressively approximating the physical case of nuclear fusion but still admitting analytical solutions. We start by considering the case of a potential describing a stepwise double symmetric barrier, then we discuss the most realistic case of a generalized Woods-Saxon potential. We investigate the tunneling phenomenon for different preparations of the wave function of the incident particle. As discussed in Ref. [28], there is a sensitive dependence of the tunneling coefficient upon the spatial spreading of the incident wave packet. While we refer to this contribution for further details, we summarize here the results relevant for the current discussion.

The incident particle is schematized via a Gaussian wave packet with positional spreading ξ (such that the position variance is ξ^2), average wave vector K, and mean energy

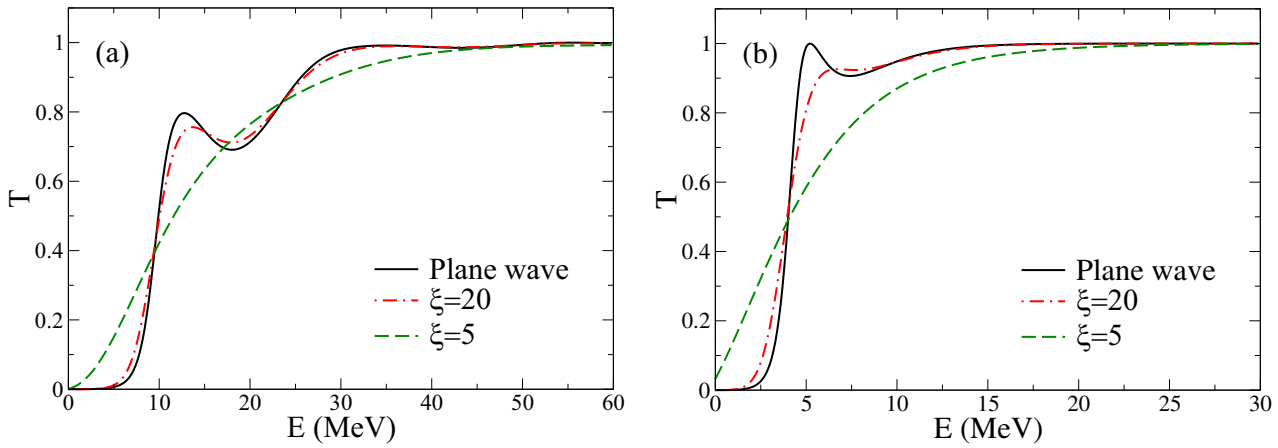

FIG. 4. (a) Tunneling coefficient versus the energy of the incident particle for a stepwise double barrier potential, with different cases of positional spreading of a Gaussian state, $\xi = 5$ (green dashed line), $\xi = 20$ (red dot-dashed line), and the case of a plane wave (black continuous line). The parameters of the potential are, with the notation used in Eq. (30), $c = 0.734$, $b = -c$, $d = c + 5$, $a = -d$, $V_0 = 5.4$, $V_1 = -40.33$. (b) Same for the case of a GWS potential, with $\lambda = 1.67$, $L = 0.5$, $U_0 = 25$, $W_0 = 56$, all lengths being expressed in fm and all energies in MeV. The reduced mass is $m = 1u$.

$\hbar^2K^2/(2m)$:

$$\psi(x,0) = \left(\frac{2}{\pi\xi^2}\right)^{1/4} e^{-(x-x_0)^2/\xi^2 + iKx}. \tag{23}$$

The corresponding wave function in wave-vector space k is

$$\begin{aligned}\varphi(k) &= \frac{1}{\sqrt{2\pi}}\int_{-\infty}^{+\infty}\psi(x,0)e^{-ikx}dx \\ &= \frac{1}{(2\pi)^{1/4}}\sqrt{\xi}e^{-\xi^2(k-K)^2/4}e^{i(K-k)x}.\end{aligned} \tag{24}$$

Therefore the probability to measure a generic wave vector k is a Gaussian function of k peaked around K:

$$P(k,K) = |\varphi(k)|^2 = \frac{\xi}{\sqrt{2\pi}}e^{-\xi^2(k-K)^2/2}. \tag{25}$$

The tunneling coefficient is therefore expressed by an integral over all wave vectors k as

$$T(K) = \int_{-\infty}^{+\infty} dk\, T\left(\frac{\hbar^2k^2}{2m}\right)P(k,K). \tag{26}$$

The reactivity is evaluated as

$$\begin{aligned}\langle\sigma v\rangle_i = &\frac{\pi\hbar^2}{\sqrt{2m^3}}\int_{-\infty}^{+\infty}dk\int_{-\infty}^{+\infty}dK\sqrt{\frac{2m}{\hbar^2k^2}} \\ &\times T\left(\frac{\hbar^2k^2}{2m}\right)P(k,K)P_i(K,\beta),\end{aligned} \tag{27}$$

where if the energy is κ distributed ($i = \kappa$) we have

$$\begin{aligned}P_\kappa(K,\beta) = &\sqrt{\frac{\hbar^2\beta}{2\pi m(\kappa+\eta)}}\frac{\Gamma(\kappa+1)}{\Gamma(\kappa+1/2)} \\ &\times\left[1+\frac{\hbar^2K^2}{2m}\frac{\beta}{\kappa+\eta}\right]^{-\kappa-1},\end{aligned} \tag{28}$$

while in the MB case ($i = \mathrm{MB}$) we have

$$P_{\mathrm{MB}}(K,\beta) = \sqrt{\frac{\hbar^2\beta}{2\pi m}}\exp\left(-\beta\hbar^2K^2/2m\right). \tag{29}$$

As discussed in Ref. [28], the reactivity for fusion processes is extremely sensitive to the spreading of the Gaussian wave packet, reaching a maximum for an intermediate value of ξ. We discuss in the following both cases of highly localized Gaussian wave packets as well as states resembling the limiting case of plane waves. Besides extending the analysis to localized states, we introduce more realistic potentials leading to tunneling processes in lieu of considering an artificial case, such as the one of Eq. (15). We first consider a stepwise double barrier potential defined as

$$V_{\mathrm{Step}}(x) = \begin{cases}0, & x < a \\ V_0, & a \leqslant x < b \\ V_1, & b \leqslant x < c \\ V_0, & c \leqslant x < d \\ 0, & x \geqslant d,\end{cases} \tag{30}$$

where $a < b < c < d$ and V_0 e V_1 are both positive defined. If $V_0 > V_1$ the potential $V(x)$ becomes a double barrier surrounding a well of depth $V_0 - V_1$. This potential admits an analytic solution for the corresponding time-independent Schrödinger equation, and transmission and reflection coefficients are calculated as described in detail in Appendix A. In Fig. 4 the dependence of the tunneling coefficient upon the energy of an incident particle is shown for two cases of positional spreading ξ and of a plane wave. A distinctive feature of the various cases is that, for large positional spreading, the curvature of the tunneling coefficient is positive at low energy, i.e., $T = T(E)$ is initially a convex function. For small positional spreading the curve becomes concave in the whole range except in a tiny region near $E = 0$.

A more realistic case, at least because of the absence of discontinuities, is provided by the generalized Woods-Saxon (GWS) potential energy for a one-dimensional system, as first

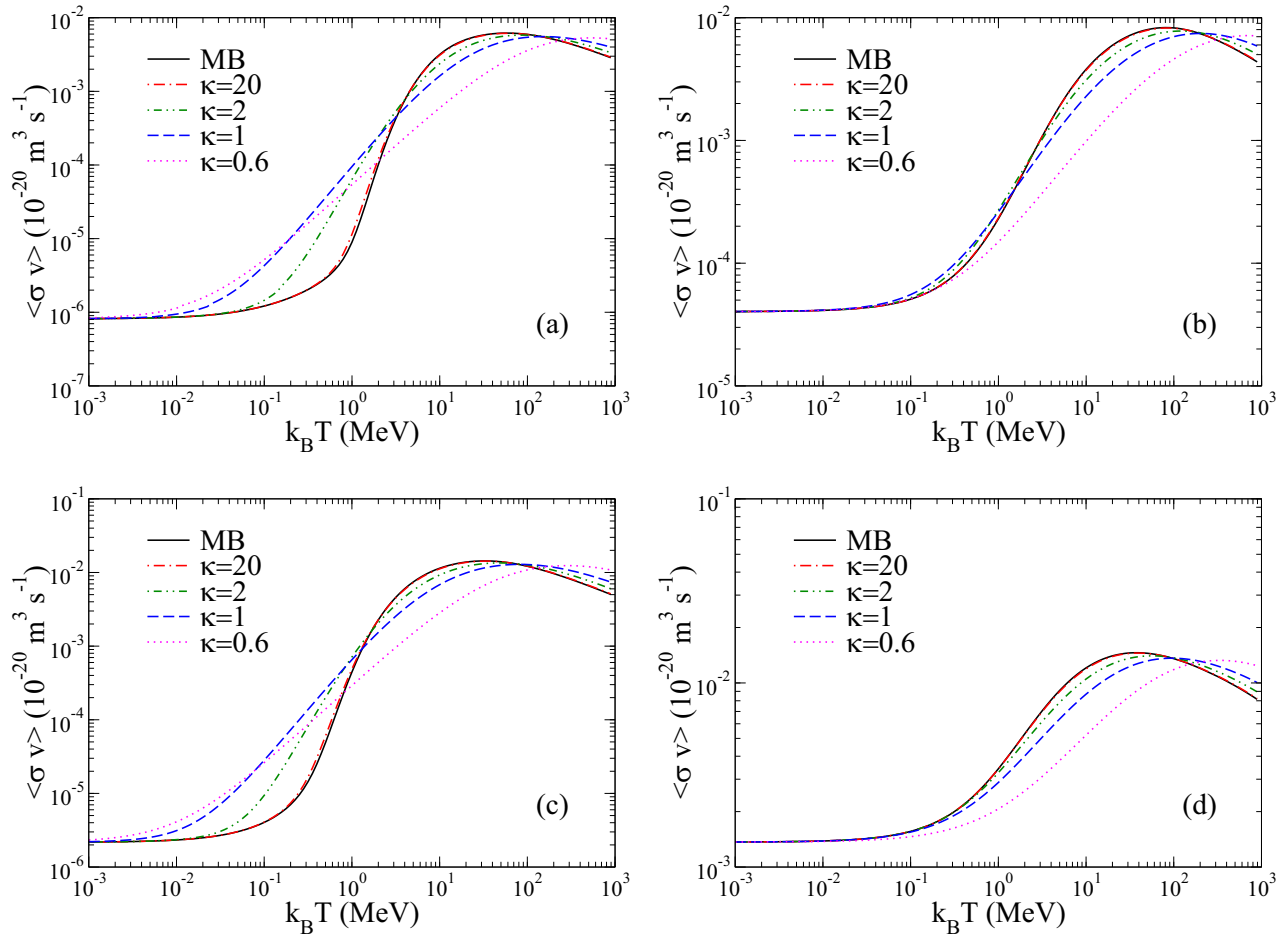

FIG. 5. Reactivity dependence on temperature for different states and energy distributions. In the top panels we show the cases of a stepwise double barrier potential, with (a) $\xi = 20$ fm and (b) $\xi = 5$ fm. In the bottom panels the corresponding cases of the GWS potential are shown for (c) $\xi = 20$ fm and (d) $\xi = 5$ fm, respectively. The various cases in each plot are relative to the choice of κ-distributed energies, with $\kappa = 0.6,\ 1,\ 2,\ 20$, and $\eta = -1/2$, and the corresponding MB distribution.

discussed in Ref. [29],

$$V_{\rm GWS}(x) = -\frac{U_0}{1+e^{(|x|-L)/\lambda}} + \frac{W_0 e^{(|x|-L)/\lambda}}{(1+e^{(|x|-L)/\lambda})^2}, \qquad (31)$$

parametrized by two characteristic lengths L and λ and two energy scales U_0 and W_0. The parameter L determines the size of the effective well, and λ is its spatial spread. The potential has a value in the origin equal to $-U_0/[1+\exp(-L/\lambda)] + W_0\exp(-L/\lambda)/[1+\exp(-L/\lambda)]^2$, while $-V_0/2 + W_0/4$ at $|x| = L$. At large distances $|x| \gg L$ the potential energy decreases as $V(x) \simeq (W_0 - V_0)\exp(-x/\lambda)$. This means that a semiqualitative difference from potential energies of interest in nuclear fusion is that the barrier experienced by the nucleons, if schematized with this potential, does not have the long range as expected for Coulomb interactions, although in a realistic plasma the latter are screened on the Debye length. We choose the set of parameters as described in the caption of Fig. 4, resulting in well depth and barrier height and width of the well comparable to those of light nuclei.

These potentials are reminiscent, in a one-dimensional setting, of the more general nucleus-nucleon interaction potential which also includes a Coulomb term inside the nucleus dictated by an assumed uniform electric charge density (here neglected) and a centrifugal term with the possibility for a scattering with nonzero impact parameter evidently absent in a one-dimensional analysis; see, for instance, Refs. [30–32]. The tunneling coefficient versus the energy of the incident particle is shown in Fig. 4 for different values of ξ. A similar phenomenon to the case of a stepwise double well is also visible, with the change of convexity depending on the values of ξ. The presence of less defined boundaries with respect to the stepwise case makes resonant tunneling less remarkable, especially in the $\xi = 20$ case, with a barely visible peak around the energy of 6 MeV.

Based on these tunneling coefficients, we can evaluate the reactivities in some examples, for simplicity limiting the analysis to the case of κ distributions. Representative results for the reactivity dependence upon the temperature are shown in Fig. 5 for both stepwise and GWS potentials. As for the tunneling coefficients, cases of Gaussian states with narrow and broad positional spreading are considered. A broad Gaussian state, with the transmission coefficient having positive curvature at low energy as shown in Fig. 4, at low temperature has a smaller reactivity for an MB distribution with respect to the corresponding κ distribution. The opposite occurs in

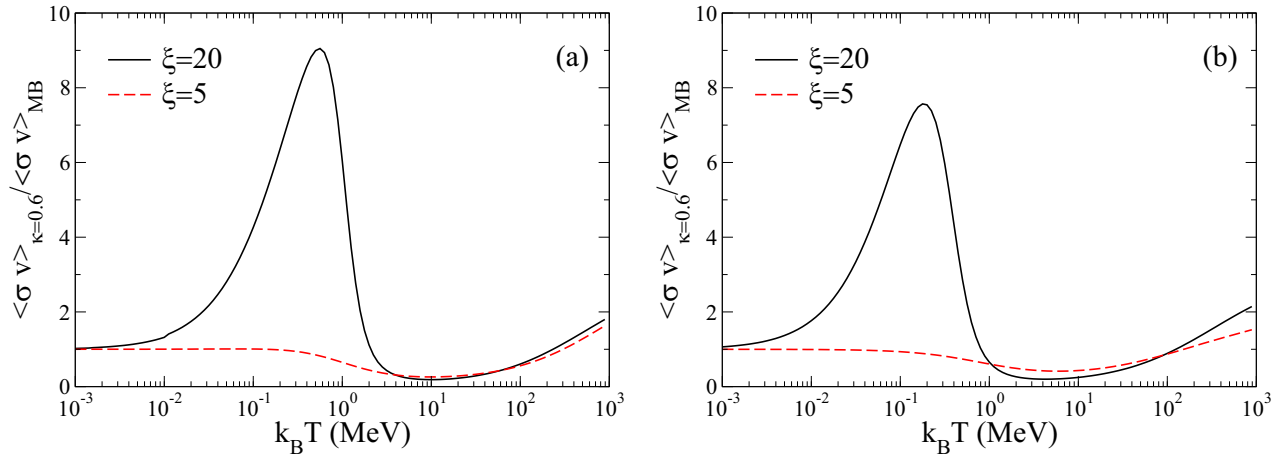

FIG. 6. Reactivity gain in using κ-distributed energies. The ratio of reactivities with the most favorable case of $\kappa = 0.6$ and the case of an MB distribution is plotted for the two positional spreadings $\xi = 5$ fm and $\xi = 20$ fm, for (a) the stepwise potential and (b) the GWS potential, the same parameters as in Fig. 4.

the case of a narrow Gaussian state in which the transmission coefficient has negative curvature in the entire range of energies. By increasing the temperature, the MB state dominates over the κ-distribution cases until the harder energy tails of the latter determine once again a gain in reactivity at even higher temperatures. To better evince the enhancement and suppression patterns, we show in Fig. 6 the ratio of reactivities between the case of $\kappa = 0.6$, the most extreme κ distribution we consider, and the case of the corresponding MB distribution. It is worth noticing that using broad Gaussian states with κ distributions at small κ allow for a gain, with respect to the MB distribution, of almost one order of magnitude, and most importantly in a range of temperatures below 1 MeV, of relevance for nuclear fusion. The analysis seems robust with respect to the choice of the potential energy, as shown by the similarity of the curves in the two cases considered.

While we plan to discuss a comprehensive analysis of realistic cases of fusion in the future, it may be worth briefly discussing the reactivity gain in using κ distributions with respect to the MB case, evaluated from empirical cross sections for fusion of deuterium-deuterium and deuterium-tritium mixtures [19]. In Fig. 7(a) this gain is plotted versus temperature in a range of interest for most of the experiments using Tokamak machines. The behavior is similar for the two mixtures. At large κ, as in the $\kappa = 10$ case, there is no gain at high temperature, while in the same temperature range it is not advantageous to use energy distributions with smaller values of κ. Significant gains are instead expected at lower temperatures. In this region of temperature there is an optimal,

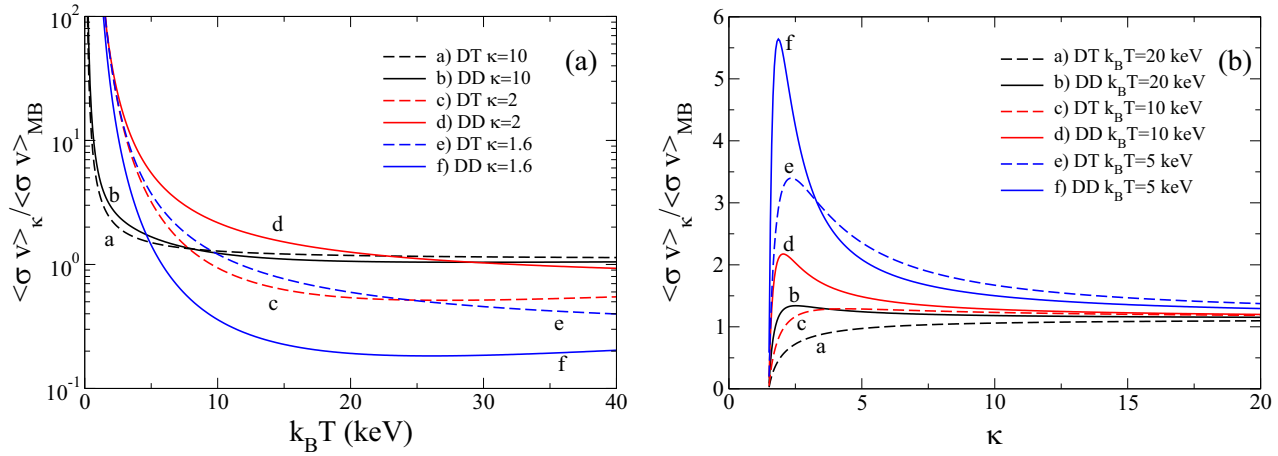

FIG. 7. Reactivity gain in using κ-distributed energies for deuterium-deuterium (continuous lines) and deuterium-tritium (dashed lines) plasmas. The ratio between reactivities with various κ distributions ($\kappa = 1.6,\ 2,\ 10$, with the $\kappa = 1.6$ case very close to the threshold value having $\eta = -3/2$ in the three-dimensional case) and the case of an MB distribution is plotted (a) versus temperature in a range of interest for the current experiments with Tokamak machines, and (b) versus the κ parameter for the three cases of temperatures of 5, 10, and 20 keV. The reactivities have been computed by using the experimental cross sections parametrized as in Ref. [19] by integrating the reactivity over energy intervals in which the interpolation is validated, 0.5–550 keV for the deuterium-tritium reaction, 0.5–5000 keV for D(d, p)T, 0.5–4900 keV for D(d, n)^{3}He (see Table IV in Ref. [19]).

intermediate value of κ maximizing the reactivity, since a too small κ creates a nearly diverging population at very low energy—see discussion around Eq. (11)—not favorable for fusion processes, see Fig. 7(b). Optimizing the value of κ yields significant reactivity gains at low and already accessible temperatures. These gains could be even substantial because, in this analysis, we do not consider the optimization with respect to the positional spreading. Moreover, the interval of energies for which the reactivity is evaluated is limited by the parametrization to a finite range, thereby resulting in conservative estimates, considering the importance of the high-energy tail for the more populated κ distribution. This analysis, based on a concrete three-dimensional situation, also confirms the general trends reported earlier on more idealized and one-dimensional models.

V. CONCLUSIONS

By using generalizations of the Maxwell-Boltzmann statistics, we have discussed a key condition to enhance the tunneling probabilities and the reactivities of nuclear fusion processes in the framework of one-dimensional potentials admitting exact solutions for the corresponding time-independent Schrödinger equation. A prominent convexity of the transmission coefficient ensures that the unavoidable overpopulation of low-energy states does not offset the effect of the high-energy tail in a κ distribution, resulting in enhanced integrated reactivity with respect to the Maxwell-Boltzmann energy distribution operating at the same effective temperature. This has been explicitly shown for bMB and κ distributions by using a convenient parametrization of the tunneling coefficient, and discussing how the latter can be approximated in more realistic but still analytically tractable potentials exhibiting tunneling.

We have presented examples of potentials for which it is advantageous to use non-Boltzmann distributions to enhance fusion reactivity. The whole parameter space for which such an advantage exists can be explored via optimization of the reactivity ratio with respect to a few parameters, three in the case of the stepwise double barrier, and four in the case of the GWS barrier, for each temperature and positional spreading. The optimization is far more complex in terms of requested numerical resources by using a more realistic potential such as, for example, a combination of Woods-Saxon and Coulomb potentials. It should be kept in mind that an overall optimization of the reactivity is what is beneficial to boost the fusion rate, therefore there is a competition between the choice of the positional spreading ξ and the κ parameter. As noticeable by comparing side by side the panels in Fig. 5, even if the gain in using a small ξ is smaller with respect to the choice of a large ξ with the same κ in the low-temperature range, the absolute reactivities are larger in the former case.

Generalizations to more realistic cases requires handling tunneling coefficients and incorporating the possible presence of states with nonzero angular momentum in a full three-dimensional treatment, as well as the effect of the confining potential on the energy distribution. The extent to which κ distributions can be realized in concrete setups is still open; however, it is expected that long-range interactions in a generic statistical system will show deviations from a Maxwell-Boltzmann distribution rigorously valid only for short-range interactions. This point is extensively discussed in Ref. [22] and corroborated by numerical simulations in the case of the Hamiltonian mean-field model [33,34]. Although we still lack evidence for κ-distributed energies in the case of genuine dynamical systems such as interacting classical gases, steps towards this direction are currently undergoing [35,36]. On the experimental side, spectroscopy of the fusion reaction products is expected to provide precise assessments of the deviation from MB distributions, as recently discussed in Ref. [37].

APPENDIX A: TUNNELING COEFFICIENT IN A STEPWISE DOUBLE WELL POTENTIAL

We report here the results for a potential made of a double well, starting with the time-independent Schrödinger equation

$$\frac{d^2}{dx^2}\phi(x) + \frac{2m}{\hbar^2}[E - V(x)]\phi(x) = 0, \tag{A1}$$

for a one-dimensional stepwise potential as defined in Eq. (30). Equation (A1) admits, for $E \geqslant 0$, a continuous and doubly degenerate spectrum. For each energy eigenvalue E there are two eigenstates $\phi_k(x)$ and $\phi_{-k}(x)$ with the positive wave vector k defined as

$$k = \sqrt{\frac{2m}{\hbar^2}E}. \tag{A2}$$

By introducing the positive wave vectors in the regions at potentials V_0 and V_1,

$$k_0 = \sqrt{\frac{2m}{\hbar^2}(V_0 - E)}, \quad k_1 = \sqrt{\frac{2m}{\hbar^2}(E - V_1)}, \tag{A3}$$

the eigenstates $\phi_k(x)$ can be expressed as

$$\phi_k(x) = (2\pi)^{-\frac{1}{2}} \begin{cases} e^{ikx} + r(k)e^{-ikx}, & x < a \\ A^+(k)e^{k_0 x} + A^-(k)e^{-k_0 x}, & a \leqslant x < b \\ B^+(k)e^{ik_1 x} + B^-(k)e^{-ik_1 x}, & b \leqslant x < c \\ C^+(k)e^{k_0 x} + C^-(k)e^{-k_0 x}, & c \leqslant x < d \\ t(k)e^{ikx}, & x \geqslant d. \end{cases} \tag{A4}$$

In this form the state $+k$ describes the stationary state of a particle coming from $x = -\infty$ with momentum $\hbar k$. The normalization is chosen in such a way that the eigenstates are orthogonalized with respect to the wave vector [38]:

$$\int_{-\infty}^{+\infty} dx\ \phi_k(x)^* \phi_{k'}(x) = \delta(k - k'). \tag{A5}$$

The particle is reflected or transmitted, respectively, with probability

$$R(k) = |r(k)|^2, \quad T(k) = |t(k)|^2. \tag{A6}$$

The reflection and transmission amplitudes $r(k)$ and $t(k)$ are determined together with the coefficients $A^{\pm}(k)$, $B^{\pm}(k)$, and $C^{\pm}(k)$ by imposing the continuity of the eigenstates and their first derivatives in the discontinuity points of the

potential. This leads to

$$t(k) = \frac{16kk_1k_0^2}{f_-(k) - f_+(k)} e^{-ik(d-a)}, \tag{A7}$$

where

$$f_\pm(k) = e^{\mp k_0(b-a)}(k_0 \pm ik)[e^{-ik_1(c-b)}(k_0 \pm ik_1)g_+(k) + e^{+ik_1(c-b)}(k_0 \mp ik_1)g_-(k)], \tag{A8}$$

$$g_\pm(k) = e^{\mp k_0(d-c)}(k_0 + ik_1)(k_0 \pm ik) - e^{\pm k_0(d-c)}(k_0 - ik_1)(k_0 \mp ik). \tag{A9}$$

The remaining coefficients are then determined as

$$A^\pm(k) = \frac{e^{\mp k_0 b}}{2k_0}[B^+(k)e^{ik_1 b}(k_0 \pm ik_1) + B^-(k)e^{-ik_1 b}(k_0 \mp ik_1)], \tag{A10}$$

$$B^\pm(k) = \frac{e^{\mp ik_1 c}}{2ik_1}[C^+(k)e^{k_0 c}(ik_1 \pm k_0) + C^-(k)e^{-k_0 c}(ik_1 \mp k_0)], \tag{A11}$$

$$C^\pm(k) = \frac{e^{\mp k_0 d}}{2k_0} t(k)e^{ikd}(k_0 \pm ik), \tag{A12}$$

$$r(k) = \frac{e^{ika}}{2ik}[A^+(k)e^{k_0 a}(ik - k_0) + A^-(k)e^{-k_0 a}(ik + k_0)]. \tag{A13}$$

APPENDIX B: INFLUENCE OF THE SHAPE OF THE BARRIER ON THE CONVEXITY OF THE TUNNELING COEFFICIENT

In this Appendix we show with a representative example how the shape of the barrier strongly influences the reactivity gain, even within the WKB approximation for which the only relevant quantity is the area of the classically forbidden region. In the case of a rectangular barrier of height V_0 and thickness a, with the particle mass and energy m and E respectively, the WKB approximation yields

$$T_r(E) \sim \exp\left[-\frac{2a}{\hbar}\sqrt{2mV_0}\left(1 - \frac{E}{V_0}\right)^{1/2}\right], \tag{B1}$$

which, in the limit $E/V_0 \to 0$, can be expanded as

$$T_r(E) \sim \left(1 + \frac{\sqrt{2mV_0}a}{\hbar}\frac{E}{V_0}\right)\exp\left(-\frac{2a}{\hbar}\sqrt{2mV_0}\right), \tag{B2}$$

a linear dependence on E in the same limit, implying no initial curvature.

If we instead consider a case with a smoother barrier, such as the following containing a Coulomb-like component:

$$V(x) = \begin{cases} V_0, & x \in [-a, +a] \\ V_0 a/|x|, & x \in (-\infty, -a] \cup [+a, \infty), \end{cases} \tag{B3}$$

we obtain, always in the WKB approximation

$$T_C(E) \sim \exp\left[-\frac{2a}{\hbar}\sqrt{\frac{2mV_0^2}{E}}\arctan\left(\sqrt{\frac{V_0}{E} - 1}\right)\right], \tag{B4}$$

where $T_C(E)$ is observed to be convex in the entire range $0 \leqslant E/V_0 \leqslant 1$. More specifically, in the $E/V_0 \to 0$ limit, the transmission coefficient is approximated as

$$T_C(E) \sim \exp\left(-\frac{\pi a}{\hbar}\sqrt{\frac{2mV_0^2}{E}}\right). \tag{B5}$$

Notice the nonanalytical dependence $T_C \propto \exp(-A/\sqrt{E})$, which implies a very soft increase and therefore a positive curvature at small values of E, i.e., $T_C(E)$ is convex. This is easily interpreted in terms of the behavior of the barriers as the energy of the impinging particle is increased. In the case of the rectangular barrier the increase in energy results in a linear decrease of the area of the classically forbidden region, therefore implying a square root dependence for the argument of the integral in the exponent of the WKB relationship. Instead, in the case of the Coulomb potential the decrease of the area of the classically forbidden region when increasing E has a stronger dependence on E, at least initially. This creates convexity of $T(E)$ at low energy. Under these conditions, as discussed in Sec. IV, spreading the energy distribution can be advantageous for enhancing the reactivity.

[1] V. I. Vysotskii, M. V. Vysotskyy, and S. V. Adamenko, Formation and application of correlated states in nonstationary systems at low energies of interacting particles, J. Exp. Theor. Phys. **114**, 243 (2012).

[2] B. Ivlev, Low-energy fusion caused by an interference, Phys. Rev. C **87**, 034619 (2013).

[3] A. V. Dodonov and V. V. Dodonov, Tunneling of slow quantum packets through the high Coulomb barrier, Phys. Lett. A **378**, 1071 (2014).

[4] A. V. Dodonov and V. V. Dodonov, Transmission of correlated Gaussian packets through a delta-potential, J. Russ. Laser Res. **35**, 39 (2014).

[5] W. Lv, H. Duan, and J. Liu, Enhanced deuterium-tritium fusion cross sections in the presence of strong electromagnetic fields, Phys. Rev. C **100**, 064610 (2019).

[6] T. X. Zhang and M. Y. Ye, Nuclear fusion with Coulomb barrier lowered by scalar field, Prog. Phys. **15**, 191 (2019).

[7] R. W. Harvey, M. G. McCoy, G. D. Kerbel, and S. C. Chiu, ICRF fusion reactivity enhancement in tokamaks, Nucl. Fusion **26**, 43 (1986).

[8] D. Nath, R. Majumdar, and M. Kalra, Thermonuclear fusion reactivities for drifting tri-Maxwellian ion velocity distributions, J. Fusion Energy **32**, 457 (2013).

[9] E. J. Kolmes, M. E. Mlodik, and N. J. Fish, Fusion yield of plasma with velocity-space anisotropy at constant energy, Phys. Plasmas **28**, 052107 (2021).
[10] K. Li, Z. Y. Liu, Y. L. Yao, Z. H. Zhao, C. Dong, D. Li, S. P. Zhu, X. T. He, and B. Qiao, Modification of the fusion energy gain factor in magnetic confinement fusion due to plasma temperature anisotropy, Nucl. Fusion **62**, 086026 (2022).
[11] H. Xie, M. Tan, D. Luo, Z. Li, and B. Liu, Fusion reactivities with drift bi-Maxwellian ion velocity distributions, Plasma Phys. Control. Fusion **65**, 055019 (2023).
[12] H. Xie, A simple and fast approach for computing the fusion reactivities with arbitrary ion velocity distributions, Comput. Phys. Commun. **292**, 108862 (2023).
[13] R. Majumdar and D. Das, Estimation of total fusion reactivity and contribution from supra-thermal tail using 3-parameter Dagum ion speed distribution, Ann. Nucl. Energy **97**, 66 (2016).
[14] R. Onofrio, Concepts for a deuterium-deuterium fusion reactor, J. Exp. Theor. Phys. **127**, 883 (2018).
[15] G. Livadiotis and D. J. McComas, Invariant kappa-distribution in space plasmas out of equilibrium, Astrophys. J. **741**, 88 (2011).
[16] D. C. Nicholls, M. A. Dopita, and R. S. Sutherland, Resolving the electron temperature discrepancies in HII regions and planetary nebulae: κ-distributed electrons, Astrophys. J. **752**, 148 (2012).
[17] D. C. Nicholls, M. A. Dopita, R. S. Sutherland, L. J. Kewey, and E. Palay, Measuring nebular temperatures: The effect of new collisions strengths with equilibrium and kappa-distributed electron energies, Astrophys. J. Suppl. Ser. **207**, 21 (2013).
[18] *Kappa Distributions: Theory and Applications in Plasmas*, edited by G. Livadiotis (Elsevier, Amsterdam, 2017).
[19] H. S. Bosch and G. M. Hale, Improved formulas for fusion cross-sections and thermal reactivities, Nucl. Fusion **32**, 611 (1992).
[20] H. Kong, H. Xie, B. Liu, M. Tan, D. Luo, Z. Li, and J. Sun, Enhancement of fusion reactivity under non-Maxwellian distributions: Effects of drift-ring-beam, slowing-down, and kappa super-thermal distributions, Plasma Phys. Control. Fusion **66**, 015009 (2024).
[21] V. P. Bhatnagar, J. Jacquinot, D. F. Start, and B. J. D. Tubbing, High-concentration minority ion-cyclotron resonance heating in jet, Nucl. Fusion **33**, 83 (1993).
[22] C. Tsallis, *Introduction to Nonextensive Statistical Mechanics: Approaching a Complex World* (Springer, New York, 2009).
[23] M. Hahn and D. Savin, A simple method for modeling collision processes in plasmas with a kappa energy distribution, Astrophys. J. Lett. **809**, 178 (2015).
[24] D. Vrinceanu, R. Onofrio, and H. R. Sadeghpour, Non-Maxwellian rate coefficients for electron and ion collisions in Rydberg plasmas: Implications for excitation and ionization, J. Plasma Phys. **86**, 845860301 (2020).
[25] G. Livadiotis, Statistical origin and properties of kappa distributions, J. Phys.: Conf. Ser. **900**, 012014 (2017).
[26] A. M. Xu, Y. C. Hu, and P. P. Tang, Asymptotic expansions for the gamma function, J. Number Theory **169**, 134 (2016).
[27] B. B. Kadomtsev and M. B. Kadomtsev, Wavefunctions of gas atoms, Phys. Lett. A **225**, 303 (1997).
[28] R. Onofrio and C. Presilla, State dependence of tunneling processes and thermonuclear fusion, Nucl. Phys. A **1043**, 122830 (2024).
[29] B. C. Lütfüoğlu, F. Akdeniz, and O. Bayrak, Scattering, bound, and quasi-bound states of the generalized symmetric Woods-Saxon potential, J. Math. Phys. **57**, 032103 (2016).
[30] M. Beckerman, Sub-barrier fusion of two nuclei, Rep. Prog. Phys. **51**, 1047 (1988).
[31] R. Vanderbosch, Angular momentum distributions in subbarrier fusion reactions, Annu. Rev. Sci. **42**, 447 (1992).
[32] A. B. Balantekin and N. Takigawa, Quantum tunneling in nuclear fusion, Rev. Mod. Phys. **70**, 77 (1998).
[33] T. Konishi and K. Kanenko, Clustered motion in symplectic couple map systems, J. Phys. A: Math. Gen. **25**, 6283 (1992).
[34] M. Antoni and S. Ruffo, Clustering and relaxation in Hamiltonian long-range dynamics, Phys. Rev. E **52**, 2361 (1995).
[35] F. Jauffred, R. Onofrio, and B. Sundaram, Scaling laws for harmonically trapped two-species mixtures at thermal equilibrium, Phys. Rev. E **99**, 022116 (2019).
[36] R. Onofrio and B. Sundaram, Relationship between nonlinearities and thermalization in classical open systems: The role of the interaction range, Phys. Rev. E **105**, 054122 (2022).
[37] A. J. Crilly, B. D. Appelbe, O. M. Mannion, W. Taitano, E. P. Hartouni, A. S. Moore, M. Gatu-Johnson, and J. P. Chittenden, Constraints on ion velocity distributions from fusion product spectroscopy, Nucl. Fusion **62**, 126015 (2022).
[38] L. Landau and E. M. Lifshitz, *Quantum Mechanics, Non-Relativistic Theory* (Pergamon Press, Oxford, 1977).